Chemical Engineering Journal 97 (2004) 131–139

Chemical Engineering Journal

www.elsevier.com/locate/cej

Modelling of catalytic monolith converters with low- and high-temperature NO_x storage compounds and differentiated washcoat

Petr Kočí [a,c], Miloš Marek [a,c,*], Milan Kubíček [b,c], Teuvo Maunula [d], Matti Härkönen [d]

[a] *Department of Chemical Engineering, Prague Institute of Chemical Technology, Technická 5, CZ-166 28 Prague, Czech Republic*
[b] *Department of Mathematics, Prague Institute of Chemical Technology, Prague, Czech Republic*
[c] *Center for Nonlinear Dynamics of Chemical and Biological Systems, Prague Institute of Chemical Technology, Prague, Czech Republic*
[d] *Kemira Metalkat, Catalyst R&D, P.O. Box 171, FIN-90101 Oulu, Finland*

Received 30 December 2002; accepted 9 May 2003

Abstract

Two types of catalytic washcoats with different properties can be present simultaneously in a monolith channel, e.g. the flat foils and the corrugated ones in metallic monolith can be individually coated with specific type of the washcoat. The model of such multiphase, differentiated NO_x storage and reduction (NSR) catalytic monolith converter has been developed. The important reactions as are the oxidation of carbon monoxide, hydrocarbons and hydrogen, the reduction of nitrogen oxides (NO_x), the water gas shift and the steam reforming reactions, the NO/NO_2 transformation, and the oxygen and NO_x storage are considered. Unknown kinetic parameters of the NSR are evaluated from transient experiments with the samples of two different types of NSR catalysts. The first catalyst is of the Pt–γ-Al_2O_3–CeO_2 type with alkali earth metals (e.g. barium) as NO_x storage components (active at lower temperature). The second one is of the PtRh–γ-Al_2O_3–CeO_2 type with both alkali earth metals and alkali metals (e.g. potassium) as NO_x storage components (active at higher temperature). Simulations of periodic lean/rich operation of the low-temperature, the high-temperature and the differentiated (combined) NSR converters are performed. The results of the computations agree well with the experimental data. The dependences of integral NO_x conversion on the lengths of the lean and rich phases and on the temperature of the inlet gas are discussed. The efficiencies of the low-temperature, the high-temperature and the differentiated NSR converters are compared at different operating conditions.

Keywords: NO_x storage catalyst; Differentiated monolith; Mathematical modelling; Non-stationary operation

1. Introduction

Legal limits for emissions of carbon monoxide, unburned hydrocarbons and nitrogen oxides (NO_x) in automotive exhaust gases are becoming more and more strict. At the same time, there is a strong pressure to lower the fuel consumption and production of carbon dioxide, which is an important greenhouse gas. Economical diesel and lean burn gasoline engines work in excess of air, which provides better efficiency and lower fuel consumption compared with gasoline engines operated at stoichiometric conditions. However, the reduction of nitrogen oxides is difficult in the excess of oxygen—the reducing components such as carbon monoxide, hydrocarbons and hydrogen are preferably oxidized by oxygen (see the reactions 1–3 in Table 1) and a large part of nitrogen oxides remains unreduced (due to low rates of the reactions 4–6 in Table 1). One possible way to lower the emissions of nitrogen oxides is then to use an NO_x storage and reduction (NSR) catalytic converter and operate it periodically [1].

The washcoat of NSR converters contains additional NO_x storage components, when compared with classical three-way catalysts (TWC). These components are mainly the compounds of the type MO, where M denotes the atom(s) of an alkali earth metal or an alkali metal, e.g. barium or potassium. They react with nitrogen oxides in the excess of oxygen, forming mainly surface nitrates (cf. the reactions 14 and 15 in Table 1). The nitrates decompose under the excess of reducing components and they are catalytically reduced to nitrogen (cf. the reactions 16–18 in Table 1). The exact reaction paths of the NSR are not clear yet. The detailed descriptions of the processes on the catalyst surface in the course of the periodic lean/rich operation have been proposed in [2–6]. In the publication [6], the competitive formation of surface hydroxyles, carbonates, nitrates and sulfates on MO sites has been reported.

* Corresponding author. Tel.: +420-22435-3104; fax: +420-23333-7335.
E-mail address: milos.marek@vscht.cz (M. Marek).

1385-8947/$ – see front matter © 2003 Elsevier B.V. All rights reserved.
doi:10.1016/S1385-8947(03)00151-7

Nomenclature

a	density of external surface area (m^{-1})
c	concentration in the flowing gas ($mol\,m^{-3}$)
c_p	molar heat capacity of the gas ($J\,mol^{-1}\,K^{-1}$)
c^s	concentration of the gas in the washcoat pores ($mol\,m^{-3}$)
c_p^s	specific heat capacity of the solid ($J\,kg^{-1}\,K^{-1}$)
D	diameter of the monolith reactor (m)
ΔH_r	standard reaction enthalpy ($J\,mol^{-1}$)
J	number of reactions
k	kinetic constant of the reaction, dimension depends on the reaction order
k_c	mass transfer coefficient ($m\,s^{-1}$)
k_h	heat transfer coefficient ($J\,m^{-2}\,K^{-1}\,s^{-1}$)
K	number of components
K_a	adsorption/inhibition constant
K^{eq}	reaction equilibrium constant
L	length of the reactor (m)
p	pressure (Pa)
R	reaction rate ($mol\,m^{-3}\,s^{-1}$)
SV	space velocity at the standard conditions (s^{-1})
t	time (s)
T	temperature of the gas (K)
T^s	temperature of the solid phase (K)
v	linear velocity ($m\,s^{-1}$)
w	relative weight of the experimental data
w_1, w_2	types of washcoat
x	parameter to be optimized
X	conversion of the component
y	molar fraction of the component
z	axial-coordinate in the monolith (m)

Greek letters

ε	macroscopic porosity of the channel
ε^s	microscopic porosity of the washcoat
λ^s	effective heat conductivity of the solid phase ($J\,m^{-1}\,K^{-1}\,s^{-1}$)
ν	stoichiometric coefficient of the component
ρ	gas density ($kg\,m^{-3}$)
ρ^s	density of the solid phase ($kg\,m^{-3}$)
τ	length of time interval (s)
φ^s	fraction of the individual type of washcoat
ψ	relative surface concentration of the stored component
Ψ	total storage capacity of the washcoat ($mol\,m^{-3}$)

Subscripts and superscripts

b	backward
eq	equilibrium
exp	experimental
f	forward
in	inlet
j	index of the reaction
k	index of the gaseous component
m	index of the surface-stored component
out	outlet
s	index of the washcoat (s = w_1, w_2)
sim	simulated
0	initial

The effective NO_x storage capacity exhibits maximum in the dependence on temperature. At lower temperatures the carbonates are preferably formed in the presence of carbon oxides and the number of MO sites available for NO_x storage decreases. At higher temperatures the surface nitrates start to decompose and the stored nitrogen oxides are released. This temperature dependence is specific for different types of NO_x storage components—typically, the compounds of alkali earth metals are active at lower temperatures and the compounds of alkali metals are active at higher temperatures. However, their combination in one catalytic washcoat may be complicated. Particularly the presence of alkali metals influences negatively the properties of the whole washcoat (sintering and deactivation of the noble metals) [1,7]. The application of differentiated metallic monolith with the flat and the corrugated foils coated individually with specific types of the washcoats—one optimized for a lower-temperature operation and another one for a higher-temperature operation (cf. Fig. 1)—has been described in Ref. [8].

The sulfates on MO sites are formed by the reaction with sulfur oxides that are produced in the engine from sulfur present in the fuel. They are difficult to decompose and they can cause gradual decrease of the NO_x storage capacity [9]. However, a new generation of NO_x storage catalysts with improved sulfur resistance has been developed [10]. When fuels with low sulfur content are used, the application of NSR converters is effective and the periodic operation, where nitrogen oxides are stored in the course of the longer

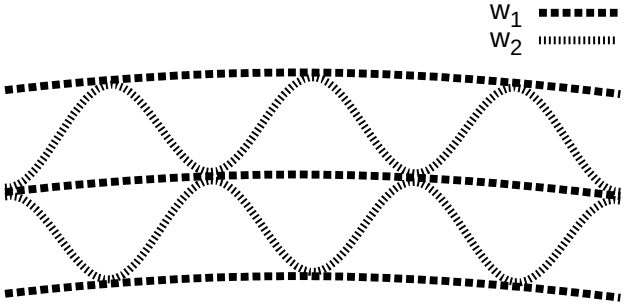

Fig. 1. Differentiated monolith schematically: a cross-section detail. The flat metallic foils are coated with the low-temperature NSR catalyst (w_1), while the corrugated foils are coated with the high-temperature NSR catalyst (w_2).

Table 1
Chemical reactions involved in the model and used kinetic relations

No.	Reaction	Kinetic expression[a]
1	$CO + \frac{1}{2}O_2 \rightarrow CO_2$	$\frac{k_1 y_{CO} y_{O_2}}{G_1}$
2	$C_3H_6 + \frac{9}{2}O_2 \rightarrow 3CO_2 + 3H_2O$	$\frac{k_2 y_{C_3H_6} y_{O_2}}{G_1}$
3	$H_2 + \frac{1}{2}O_2 \rightarrow H_2O$	$\frac{k_3 y_{H_2} y_{O_2}}{G_1}$
4	$CO + NO \rightarrow CO_2 + \frac{1}{2}N_2$	$k_4 y_{CO} y_{NO}^{0.5}$
5	$C_3H_6 + 9NO \rightarrow 3CO_2 + 3H_2O + \frac{9}{2}N_2$	$k_5 y_{C_3H_6} y_{NO}^{0.5}$
6	$H_2 + NO \rightarrow H_2O + \frac{1}{2}N_2$	$k_6 y_{H_2} y_{NO}^{0.5}$
7	$NO + \frac{1}{2}O_2 \rightleftarrows NO_2$	$\frac{k_7^f y_{NO} y_{O_2}^{0.5} - k_7^b y_{NO_2}}{G_2}$
8	$CO + H_2O \rightleftarrows CO_2 + H_2$	$k_8(y_{CO} y_{H_2O} - (y_{CO_2} y_{H_2})/K_8^{eq})$
9	$C_3H_6 + 3H_2O \rightleftarrows 3CO + 6H_2$	$k_9(y_{C_3H_6} y_{H_2O} - (y_{CO}^3 y_{H_2}^6)/(K_9^{eq} y_{H_2O}^2))$
10	$Ce_2O_3 + \frac{1}{2}O_2 \rightarrow 2CeO_2$	$k_{10} \Psi_{O_2} y_{O_2} (\psi_{O_2}^{eq} - \psi_{O_2})$
11	$2CeO_2 + CO \rightarrow Ce_2O_3 + CO_2$	$k_{11} \Psi_{O_2} y_{CO} \psi_{O_2}$
12	$18CeO_2 + C_3H_6 \rightarrow 9Ce_2O_3 + 3CO_2 + 3H_2O$	$k_{12} \Psi_{O_2} y_{C_3H_6} \psi_{O_2}$
13	$2CeO_2 + H_2 \rightarrow Ce_2O_3 + H_2O$	$k_{13} \Psi_{O_2} y_{H_2} \psi_{O_2}$
14[b]	$2NO_2 + \frac{1}{2}O_2 + MO \rightarrow M(NO_3)_2$	$k_{14} \Psi_{NO_x} y_{NO_2} (\psi_{NO_x}^{eq} - \psi_{NO_x})$
15[b]	$2NO + \frac{3}{2}O_2 + MO \rightleftarrows M(NO_3)_2$	$k_{15} \Psi_{NO_x} y_{NO} (\psi_{NO_x}^{eq} - \psi_{NO_x})$
16[b]	$M(NO_3)_2 + 5CO \rightarrow N_2 + 5CO_2 + MO$	$k_{16} \Psi_{NO_x} y_{CO} \psi_{NO_x}$
17[b]	$M(NO_3)_2 + \frac{5}{9}C_3H_6 \rightarrow N_2 + \frac{5}{3}CO_2 + \frac{5}{3}H_2O + MO$	$k_{17} \Psi_{NO_x} y_{C_3H_6} \psi_{NO_x}$
18[b]	$M(NO_3)_2 + 5H_2 \rightarrow N_2 + 5H_2O + MO$	$k_{18} \Psi_{NO_x} y_{H_2} \psi_{NO_x}$

[a] Inhibition terms are: $G_1 = (1 + K_{a1} y_{CO} + K_{a2} y_{C_3H_6})^2 (1 + K_{a3} y_{CO}^2 y_{C_3H_6}^2)(1 + K_{a4} y_{NO_x}^{0.7}) T$, $G_2 = 1 + K_{a5} y_{NO} + K_{a6} y_{O_2}^{0.5} + K_{a7} y_{NO_2}$.

[b] $M = M^{II}$, $2M^{I}$. Different NO_x storage capacities (Ψ_{NO_x}) and kinetic dependences ($\psi_{NO_x}^{eq}, k_{14}, \ldots, k_{18}$) are used for the M^{II} and M^{I} sites that are present simultaneously.

lean period (excess of oxygen, low fuel consumption) and then reduced within the short rich period (excess of reducing species, injection of a rich fuel mixture), can result in high integral NO_x conversions [8].

In this paper we present a mathematical model of the monolith with differentiated washcoat. Then we discuss the experimental work and the evaluation of unknown kinetic parameters from the experimental data. We continue with the comparison of experimental and modelled NO_x concentrations at the outlet of the monolith. The model is then used for the study of effects of parameters of periodic lean/rich operation (the inlet gas temperature and the lengths of the lean and rich phases) on the integral NO_x conversion. Spatiotemporal concentration and temperature patterns in the low-temperature, the high-temperature and the differentiated monoliths are discussed and the performances of all three types of catalytic monolithic converters are finally compared.

2. Model of differentiated catalytic monolith

A spatially pseudo-1D, multiphase model of an adiabatic catalytic monolith has been developed. It accounts for the configuration of the differentiated monolith, where two different types of the washcoats (denoted by the superscripts w_1 and w_2) can be present simultaneously in each channel. Mass and enthalpy balances are then written separately for two solid phases with different properties (e.g. reaction kinetics). Mass balances in the flowing gas (1), in the washcoat pores (2) and on the catalyst surface (3) are considered:

$$\frac{\partial c_k(z,t)}{\partial t} = -\frac{\partial (v c_k)}{\partial z} - k_c(z)\frac{a^{w_1}}{\varepsilon}(c_k - c_k^{w_1}) - k_c(z)\frac{a^{w_2}}{\varepsilon}(c_k - c_k^{w_2}) \quad (1)$$

$$\varepsilon^s \frac{\partial c_k^s(z,t)}{\partial t} = k_c(z)\frac{a^s}{\varphi^s(1-\varepsilon)}(c_k - c_k^s) + \sum_{j=1}^{J} \nu_{k,j} R_j^s, \quad s = w_1, w_2 \quad (2)$$

$$\frac{\partial \psi_m^s(z,t)}{\partial t} = \frac{1}{\Psi_m^s} \sum_{j=1}^{J} \nu_{m,j}^{\psi} R_j^s, \quad s = w_1, w_2 \quad (3)$$

Enthalpy balances in the flowing gas (4) and in the solid phases (5) are of the form as

$$\rho c_p \frac{\partial T(z,t)}{\partial t} = -v\rho c_p \frac{\partial T}{\partial z} - k_h(z)\frac{a^{w_1}}{\varepsilon}(T - T^{w_1}) - k_h(z)\frac{a^{w_2}}{\varepsilon}(T - T^{w_2}) \quad (4)$$

$$\rho^s c_p^s \frac{\partial T^s(z,t)}{\partial t} = \lambda^s \frac{\partial^2 T^s}{\partial z^2} - \sum_{j=1}^{J} \Delta H_{r,j} R_j^s + k_h(z)\frac{a^s}{\varphi^s(1-\varepsilon)}(T - T^s), \quad s = w_1, w_2 \quad (5)$$

The values of mass and heat transfer coefficients along the monolith channel ($k_c(z)$ and $k_h(z)$, respectively) have been calculated from the correlations [11].

Boundary conditions at the inlet ($z = 0$) and at the outlet ($z = L$) of the monolith are

$$T(0,t) = T_{in}(t) \quad (6)$$

$$\frac{\partial T^s(0,t)}{\partial z} = 0, \quad s = w_1, w_2 \quad (7)$$

$$c_k(0,t) = c_{in,k}(t), \quad k = 1, \ldots, K \quad (8)$$

$$\frac{\partial T^s(L,t)}{\partial z} = 0, \quad s = w_1, w_2 \quad (9)$$

A complex set of important components of automobile exhaust gases and their catalytic reactions is employed. The considered reactions and their kinetics are listed in Table 1. The Langmuir–Hinshelwood–Voltz relations have been used for the combustion of carbon monoxide, hydrocarbons (here represented by propylene) and hydrogen (the reactions 1–3), empirical power-law kinetics for the reduction of nitrous oxide (the reactions 4–6) and equilibrium approach for the water gas shift and steam reforming (the reactions 8 and 9). Similar description has been used earlier, cf., e.g. [12]. The kinetics of reversible oxidation of nitrous oxide to nitric oxide (the reaction 7) has been derived from the kinetic study [13]. Non-stationary kinetic relations have been used for the description of the oxygen and NO_x storage properties (the reactions 10–18), by analogy with the model proposed in Ref. [14]. The temperature dependence of the effective storage capacity (i.e. $\psi^{eq}(T)$) has been included in the way similar to Ref. [15]. The finite difference method of the Crank-Nicolson type with quasi-linearization of reaction terms has been used for numerical solution of the system of partial differential Eqs. (1)–(5) with the boundary conditions (6–9).

3. Experiments and evaluation of parameters

3.1. Experimental work

Two samples of non-differentiated metallic monoliths coated with γ-Al_2O_3 based NSR catalysts have been used in the experiments. The catalyst w_1 with platinum (4.9 g dm^{-3}) as an active catalytic metal contains only low-temperature NO_x storage compounds of alkali earth metals (e.g. barium, lanthanum) of the type $M^{II}O$. The catalyst w_2 with platinum and rhodium (10:1, 3.5 g dm^{-3}) as active catalytic metals contains both alkali earth metals and high-temperature NO_x storage compounds of alkali metals (e.g. potassium) of the type M^{I}_2O. There is also a certain amount of oxygen storage compounds (e.g. CeO_2) present in both NSR catalysts. It is known that cerium acts as the catalyst in the water gas shift and steam reforming reactions [16]. These reactions are beneficial especially during the rich phase, since hydrogen (an efficient NO_x reductant) is produced in situ [17].

Exhaust gases at the inlet of the converter have been simulated by the synthetic gas mixtures with defined compositions and flow rates. Carbon monoxide, propylene and hydrogen have been used as NO_x reductants. Hydrothermally aged (700 °C, 20 h) monolith samples ($L = 7.5$ cm, $D = 14$ mm, 500 cpsi) have been examined in an isothermal laboratory reactor. The space velocity of the gas has been kept constant in the range 30 000–120 000 h^{-1} in the course of each experiment. Concentration responses behind the NSR converter have been recorded by analyzers of nitrogen oxides, carbon monoxide, hydrocarbons and oxygen with the frequency 1 s^{-1}. The cycles including longer lean phase and short rich phase, simulating lean burn gasoline engine conditions without sulfur oxides, have been repeated seven times in the temperature range 200–600 °C (cf. Fig. 2). The concentrations in the course of short rich peaks have been measured also in the blank experiments to determine the influence of the mixing and the transport delay in the inlet lines. The measurements of long lean phases until saturation (cf. Fig. 3) have been performed at different temperatures to find the temperature dependence of the effective NO_x storage capacity (i.e. $\psi^{eq}_{NO_x}(T)$).

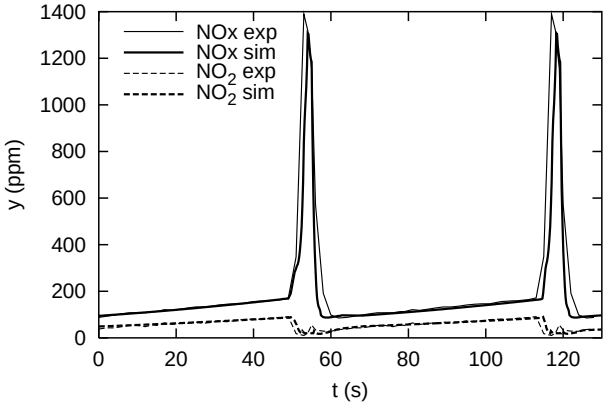

Fig. 2. The comparison of experimental and simulated outlet NO_x concentrations. Stable, isothermal, periodic lean/rich operation at 250 °C. The low-temperature catalyst (w_1), SV = 30 000 h^{-1}, $\tau_{lean} = 60$ s, $\tau_{rich} = 5$ s (effects of mixing in the inlet lines included). Inlet gas composition: $y_{O_2,lean} = 7\%$, $y_{CO,lean} = 0.3\%$, $y_{NO,lean} = 500$ ppm, $y_{O_2,rich} = 0.1\%$, $y_{CO,rich} = 8\%$, $y_{NO,rich} = 1500$ ppm, $y_{H_2O} = 10\%$, $y_{CO_2} = 10\%$.

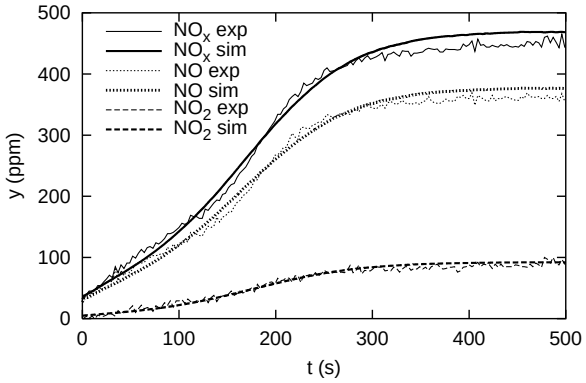

Fig. 3. The comparison of experimental and simulated outlet NO_x concentrations. A long lean phase until saturation. The high-temperature catalyst (w_2), SV = 30 000 h^{-1}, T = 500 °C (isothermal). Inlet gas composition: y_{O_2} = 7%, y_{NO} = 470 ppm, y_{NO_2} = 0, y_{CO} = 0.3%, $y_{C_3H_6}$ = 0, y_{H_2} = 0, y_{H_2O} = 10%, y_{CO_2} = 10%. The initial conditions: a completely reduced surface ($\psi_{0,NO_x}(z) = 0$).

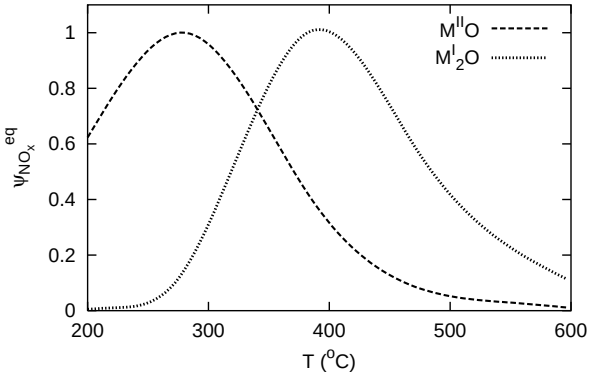

Fig. 4. Temperature dependences of NO_x storage capacity for the $M^{II}O$ sites (the low-temperature NSR catalyst, w_1) and for the M^I_2O sites (the high-temperature NSR catalyst, w_2).

3.2. Evaluation of kinetic parameters

The weighted least squares method has been used in the evaluation of unknown kinetic parameters separately for the low-temperature ($M^{II}O$) and the high-temperature (M^I_2O) NO_x storage components in the respective types of the washcoats. The NO_x storage capacities (Ψ_{NO_x} and $\psi^{eq}_{NO_x}(T)$ in Table 1) and the rate constants for the NO_x storage ($k_{14}(T)$ and $k_{15}(T)$ in Table 1) have been evaluated from the measurements of the long lean phases until NO_x saturation. The rate constants for the reduction of the stored NO_x ($k_{16}(T), \ldots, k_{18}(T)$ in Table 1) have been then evaluated from the measurements of periodic lean/rich operation at different conditions. The following objective function has been minimized by the simplex method [18]:

$$S(\vec{x}) = \sum_i \sum_{k=1}^{K} \{w_k (y^{exp,i}_{out,k} - y^{sim,i}_{out,k}(\vec{x}))^2\} \quad (10)$$

Here $\vec{x}$ are the parameters to be evaluated, i is the index of the data point in the time sequence obtained in the course of the experiment and w_k is the corresponding weight for the component k. The weights have been chosen in dependence on the relative errors of measurements and on the relative importance of the experiment and the component. Zero weight ($w_k = 0$) has been used in cases where the effect of respective component is not considered for the evaluation of given parameters [19,20]. The overall optimization for several experiments at different temperatures has been performed to evaluate the activation energies of the reactions. After that, the optimized kinetic parameters have been kept constant throughout the entire simulation study. The simulation results are compared with experimental data in Figs. 2 and 3. We can observe excellent agreement among the measured and simulated data both for the dynamic (Fig. 2) and the saturation experiments (Fig. 3). Total effective NO_x storage capacities (Ψ_{NO_x}, related to the volume of the washcoat) were 150 mol m^{-3} for the low-temperature NSR catalyst ($M^{II}O$ sites only) and 20 and 150 mol m^{-3} for the high-temperature NSR catalyst ($M^{II}O$ and M^I_2O sites, respectively). The evaluated temperature dependences of the relative NO_x storage capacities ($\psi^{eq}_{NO_x}(T)$) for the $M^{II}O$ and M^I_2O sites are shown in Fig. 4. It can be seen from this figure that the used combined low- and high-temperature NO_x storage components provide sufficiently high NO_x storage capacity in the temperature range 200–500 °C.

4. Simulation results and discussion

The developed model fitted to experimental data enables detailed studies of spatiotemporal temperature and concentration patterns in the monolith and also the optimization of parameters of periodic lean/rich operation (e.g. the lengths of the lean and rich phases) with respect to maximum overall, time-averaged NO_x conversion. The results of the study of dynamic behavior of the low-temperature, the high-temperature and the differentiated adiabatic NSR converters (L = 15 cm) in the course of periodic lean/rich operation are presented below. The composition of the inlet gas used in the simulations is given in Table 2; ideal step changes between the lean and the rich concentration levels have been considered.

Table 2
Inlet gas composition (balance N_2) used in the simulations in the lean and the rich phase (space velocity SV=30 000 h^{-1})

Component	Lean mixture	Rich mixture
CO (%)	0.3	5
C_3H_6 (ppm)	200	1000
O_2 (%)	7	0.3
NO (ppm)	450	1050
NO_2 (ppm)	50	50
CO_2 (%)	10	10
H_2O (%)	10	10

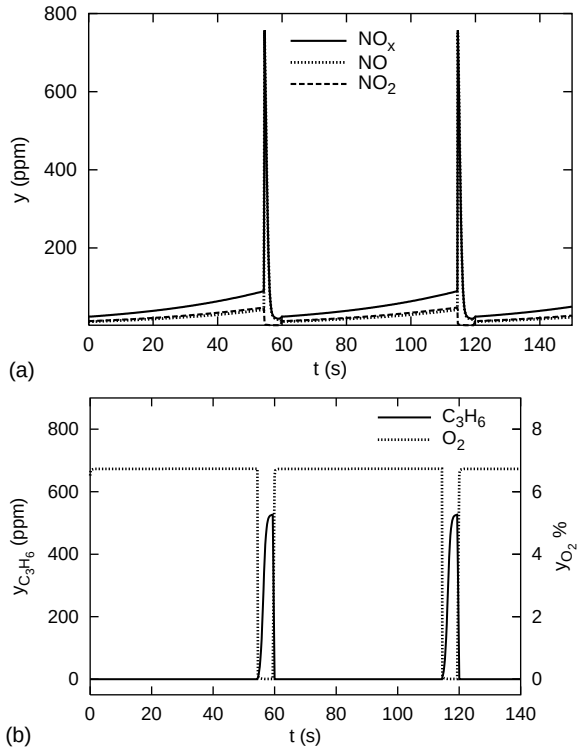

Fig. 5. Simulated steady outlet concentrations in the course of periodic lean/rich operation of the adiabatic, low-temperature NSR converter. $\tau_{lean} = 55\,s$, $\tau_{rich} = 5\,s$, $T_{in} = 350\,^{\circ}C$, the inlet concentrations are given in Table 2: (a) outlet concentrations of NO, NO_2, and NO_x; (b) outlet concentrations of O_2 and C_3H_6.

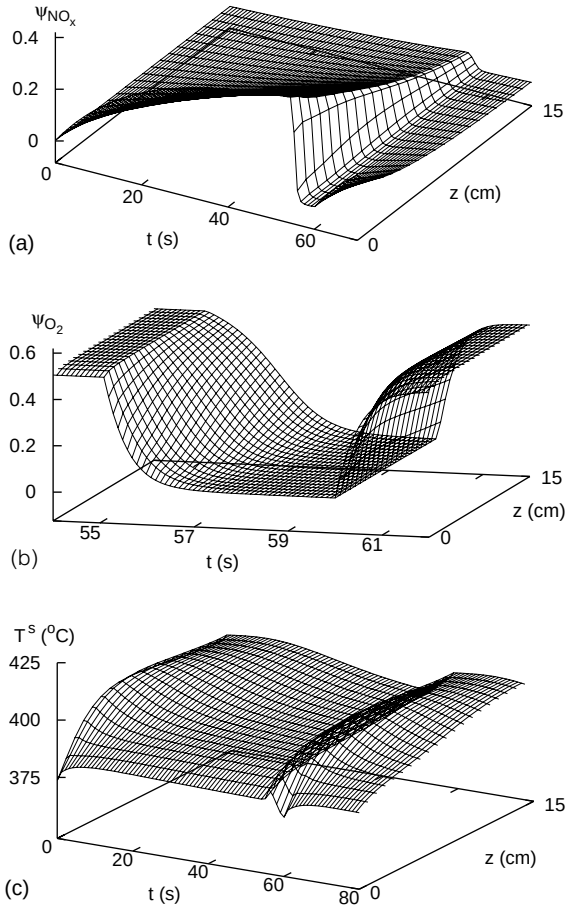

Fig. 6. Simulated spatiotemporal profiles of the adiabatic monolith in the course of periodic lean/rich operation. The low-temperature NSR converter, $\tau_{lean} = 55\,s$, $\tau_{rich} = 5\,s$, $T_{in} = 350\,^{\circ}C$, the inlet concentrations are given in Table 2: (a) concentration of the stored NO_x (ψ_{NO_x}); (b) concentration of the stored O_2 (ψ_{O_2}, a detail within the rich phase); (c) temperature of the monolith (T^s).

Let us discuss first the course of periodic lean/rich operation at an intermediate temperature in general. It is qualitatively independent of the employed NO_x storage compounds. The typical development of the outlet concentrations in the course of periodic lean/rich operation is shown in Fig. 5. Nitrogen oxides are stored on the washcoat surface during the lean phase and the MO storage centers are gradually saturated from the front to the rear part of the converter, as can be seen in Fig. 6a. Concurrently, the outlet concentrations of nitrogen oxides increase slowly (cf. Fig. 5a). To avoid the undesired breakthrough of nitrogen oxides, a short enrichment of the inlet gas is applied. In the excess of reducing components (carbon monoxide, hydrocarbons and hydrogen), the stored nitrogen oxides are reduced and the surface is regenerated (cf. Fig. 6a). Certain amount of unburned hydrocarbons and carbon monoxide is also consumed by the reactions with the stored oxygen (cf. the ψ_{O_2} profile in Fig. 6b). The conversions of carbon monoxide and hydrocarbons under the lean conditions are almost complete, while their emissions are observed within the rich phase (cf. Fig. 5b).

The example of spatiotemporal temperature profile in the adiabatic monolith in the course of the periodic lean/rich operation is given in Fig. 6c. Due to the high concentrations of combustibles and exothermicity of the reactions, an additional heat is generated within the rich phase and the temperature of the monolith increases. Subsequently, in the course of the lean phase, the temperature of the monolith decreases back to its original value, gradually from the front to the rear part of the reactor. The almost flat temperature profile at the end of the lean phase in Fig. 6c indicates that carbon monoxide and hydrocarbons are burned off very fast—the heat is produced only close to the inlet of the reactor and then transported by convection of the gas (4) and conduction in the solid phase (5).

An important parameter of the periodic lean/rich operation is the length of the rich phase. If the rich phase is too short then the stored nitrogen oxides are not fully reduced. Thus the number of free storage sites for the next lean phase is lower and NO_x conversion decreases. Only the front part of the reactor then effectively participates in the NSR operation. Such situation is depicted in Fig. 7. On the other hand, as soon as the NO_x storage capacity is fully regenerated, then the application of longer rich phase is pointless—it increases the fuel consumption and brings no improvement to NO_x storage efficiency. The example of the effect of the length

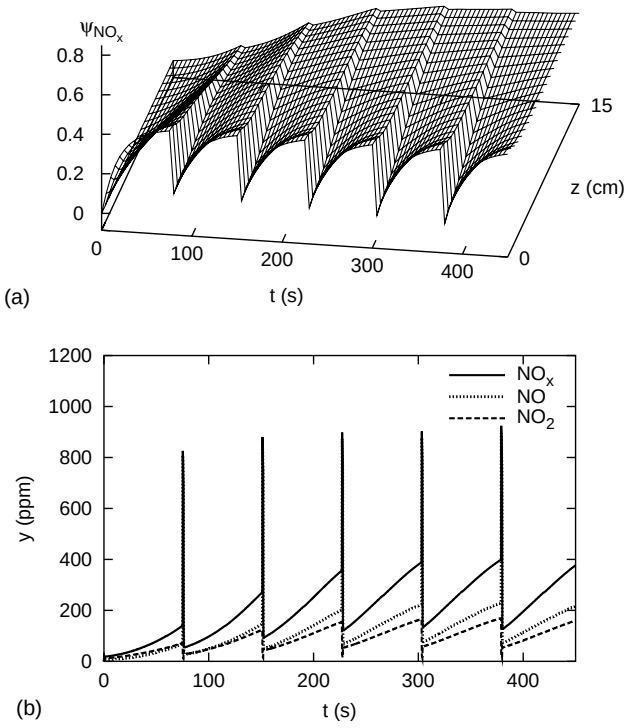

Fig. 7. Simulated periodic lean/rich operation with a very short rich phase. The low-temperature, adiabatic NSR converter, $\tau_{lean} = 75\,s$, $\tau_{rich} = 1\,s$, $T_{in} = 350\,^{\circ}C$, the inlet concentrations are given in Table 2. The initial conditions: a completely reduced surface ($\psi_{0,NO_x}(z) = 0$), $T_0^s(z) = 350\,^{\circ}C$: (a) spatiotemporal concentration profile of the stored NO_x (ψ_{NO_x}); (b) the corresponding NO_x concentrations in the gas at the outlet of the reactor.

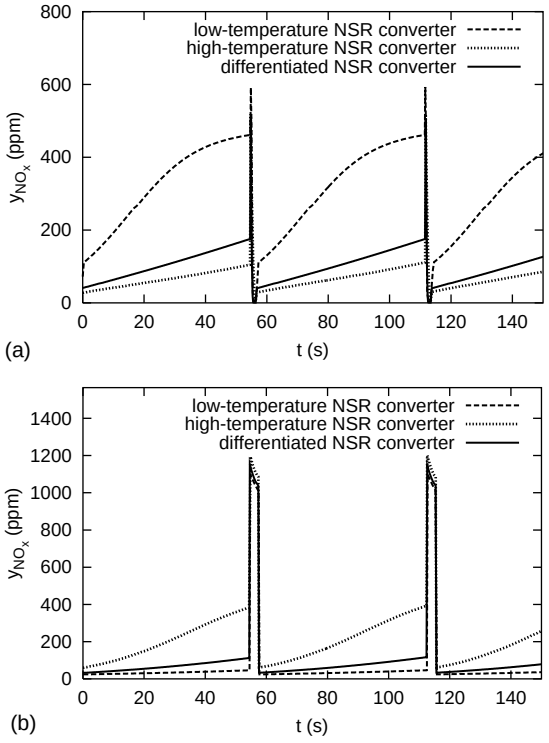

Fig. 9. The comparison of steady outlet NO_x concentrations from the low-temperature, the high-temperature and the differentiated adiabatic NSR converters. A simulated periodic lean/rich operation, the inlet concentrations are given in Table 2: (a) high-temperature operation, $T_{in} = 450\,^{\circ}C$, $\tau_{lean} = 55\,s$, $\tau_{rich} = 2\,s$; (b) low-temperature operation, $T_{in} = 270\,^{\circ}C$, $\tau_{lean} = 55\,s$, $\tau_{rich} = 3\,s$.

of the rich phase on the integral NO_x conversion is shown in Fig. 8.

Let us look now in more detail on the differences in the NO_x storage on $M^{II}O$ and M^{I}_2O sites. The surface nitrates are not stable at higher temperatures and thus the NO_x storage capacity considerably decreases. It can be seen from Fig. 4 that particularly the NO_x storage capacity of $M^{II}O$ sites (compounds of alkali earth metals) is very low at higher temperatures. Hence an early breakthrough of NO_x occurs

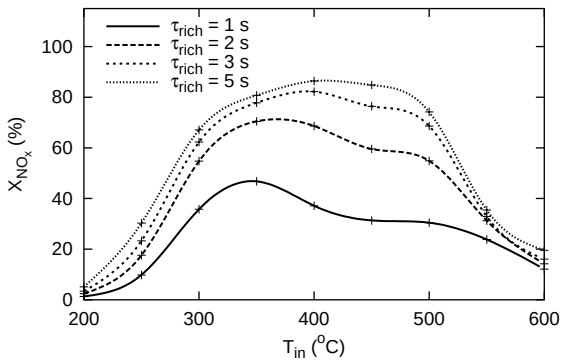

Fig. 8. The dependence of the integral NO_x conversion on the length of the rich phase for different temperatures of the inlet gas (T_{in}). A simulated periodic lean/rich operation of the adiabatic, high-temperature NSR converter. $\tau_{lean} = 95\,s$, the inlet concentrations are given in Table 2.

in the low-temperature NSR converter at higher temperatures, as can be seen in Fig. 9a. On the contrary, the M^{I}_2O sites (compounds of alkali metals) in the high-temperature NSR catalyst preserve their NO_x storage capacity up to high temperatures (cf. Figs. 4 and 9a).

However, the high-temperature NSR catalyst is not suitable for the operation in the range of low temperatures. Under these conditions the NO_x storage capacity of alkali metals (M^{I}_2O sites) is not fully activated due to blocking by the surface carbonates (cf. Fig. 4). Furthermore, the high-temperature NSR catalyst exhibits lower activity of noble metals (caused by the presence of alkali metals) and thus higher light-off temperature. The concentrations of nitrogen oxides at the outlet of the low- and the high-temperature NSR converters in the course of periodic lean/rich operation at a lower temperature are compared in Fig. 9b.

The operation in a wide temperature range can be then achieved by the use of differentiated NSR converter, which combines the low- and high-temperature NSR catalysts. Let us discuss the case, where the fractions of the washcoat types in the differentiated NSR converter are $\varphi^{w1} = 0.4$ (the flat foils coated with the low-temperature catalyst) and $\varphi^{w2} = 0.6$ (the corrugated foils coated with the high-temperature catalyst). Such converter exhibits a sufficient NO_x storage capacity at higher temperatures and an

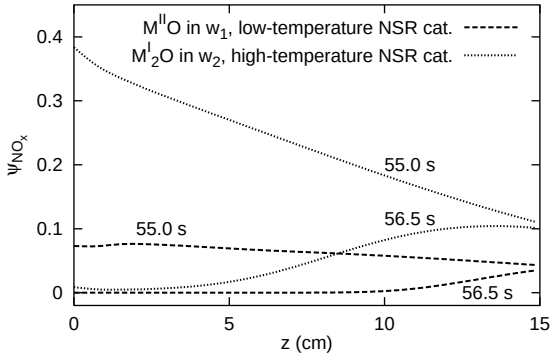

Fig. 10. Simulated concentration profiles of the stored NO_x (ψ_{NO_x}) in the course of periodic lean/rich operation of the adiabatic, differentiated NSR converter: $T_{in} = 450\,^{\circ}C$, $\tau_{lean} = 55\,s$, $\tau_{rich} = 3\,s$. The profiles at the end of the lean phase ($t = 55.0\,s$) and in the middle of the rich phase ($t = 56.5\,s$) are shown. The inlet concentrations are given in Table 2.

improved performance at lower temperatures when compared with the high-temperature NSR converter (cf. Fig. 9).

Spatial concentration profiles of the stored nitrogen oxides in the course of lean/rich operation of the differentiated monolith at a high temperature are given in Fig. 10. In this case the contribution of the low-temperature NSR catalyst (w_1, $M^{II}O$ sites only) to the overall NO_x storage capacity of the differentiated converter is minor and the efficient lean/rich operation is enabled by the presence of the M^{I}_2O sites in the high-temperature NSR catalyst (w_2). Significant spatial concentration gradients of the stored nitrogen oxides can be seen within the rich phase (cf. Fig. 10) as the reduction of the stored nitrogen oxides proceeds from the inlet to the rear part of the monolith.

Temperature profiles in the differentiated monolith and the respective carbon monoxide concentration profiles in the course of the simulated light-off are depicted in Fig. 11. The low-temperature catalyst ignites first and generates a significant amount of heat, causing earlier light-off of the high-temperature catalyst (i.e. at lower temperatures of the inlet gas). Moreover, the low-temperature NSR catalyst considerably improves the overall NO_x storage capacity of the differentiated NSR converter at lower temperatures (cf. Fig. 4).

Typical concentration profiles of hydrogen under lean conditions in the differentiated monolith are given in Fig. 12. Hydrogen is produced in the front part of the reactor, by water gas shift and steam reforming reactions from carbon monoxide, hydrocarbons and water. The concentrations of carbon monoxide and hydrocarbons rapidly decrease along the monolith as they are consumed by a fast oxidation under the excess of oxygen (cf. Fig. 11b). Thus hydrogen is not produced any more and it is burned off in the excess of oxygen. It can be seen from Fig. 12 that the used high-temperature NSR catalyst exhibits a higher activity for the water gas shift and steam reforming reactions—it is caused by the presence of Rh, which is known to be an efficient catalyst for these reactions [17].

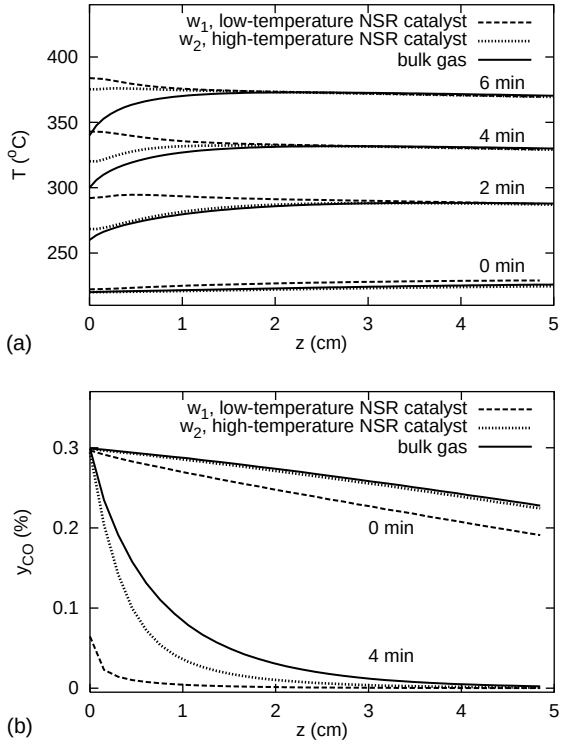

Fig. 11. Temperature and concentration profiles of the front part (1/3) of the monolith in the course of simulated light-off of the adiabatic, differentiated NSR converter. Temperature ramp in the inlet gas (T_{in} increases with the rate of $20\,^{\circ}C\,min^{-1}$). The lean mixture (cf. Table 2). (a) the temperature profiles are given at the times 0, 2, 4 and 6 min; (b) the respective CO concentration profiles are given at the times 0 and 4 min.

The examples of the results of simulation study focused on the comparison of overall integral NO_x conversions in different types of NSR converters at different operating conditions of periodic lean/rich operation are shown in Figs. 8 and 13. The comparison of integral NO_x conversions for the low-temperature, the high-temperature and the differentiated NSR converters (cf. Fig. 13) demonstrate that the combination of the low- and the high-temperature NSR catalysts in the differentiated monolith can significantly extend the range of operation conditions of NSR converters.

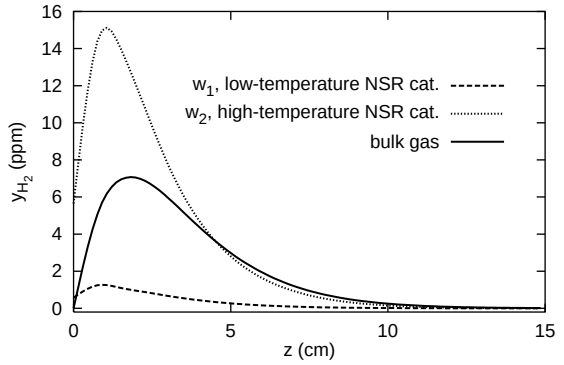

Fig. 12. Simulated concentration profiles of H_2 in the adiabatic, differentiated NSR converter: $T_{in} = 350\,^{\circ}C$, the lean mixture (cf. Table 2).

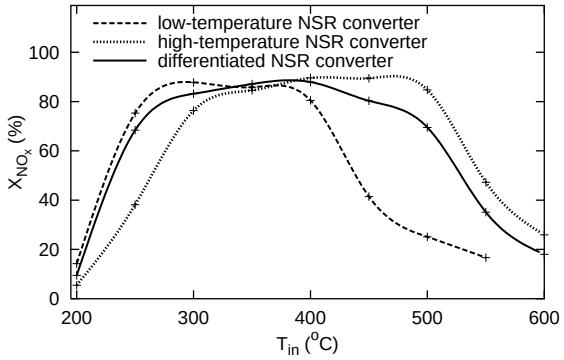

Fig. 13. The comparison of the efficiencies of the low-temperature, the high-temperature and the differentiated adiabatic NSR converters—dependencies of the integral NO_x conversion on the temperature of the inlet gas (T_{in}). A simulated periodic lean/rich operation, $\tau_{lean} = 55\,s$, $\tau_{rich} = 3\,s$, the inlet concentrations are given in Table 2.

5. Conclusions

The mathematical model for description and/or prediction of dynamic behavior of differentiated NSR monolith converter has been developed on the basis of evaluation of experimental data. The simulation of the activity of combined NO_x storage components has been described for the first time. It demonstrates that their simultaneous use can significantly extend the range of operation conditions of NSR converters. Experimental studies of evolutions of spatially 2D temperature profiles in catalytic monolith reactors [21] and simulations of adsorber-reactor systems with adaptive control [22] demonstrated earlier that a proper dynamic control can increase the time averaged conversions of NO_x and combustibles, even under cold-start conditions. The periodic lean/rich operation and the differentiation of washcoat in NSR monoliths are other possibilities to improve the efficiency of automobile exhaust gas converters. The developed model thus forms a useful tool for studies of the influence of different operation conditions and monolith configurations on the performance of differentiated NSR converters.

Acknowledgements

This work has been partially supported by the project MSM 223400007 of Czech Ministry of Education.

References

[1] N. Takahashi, H. Shinjoh, T. Iijima, T. Suzuki, K. Yamazaki, K. Yokota, H. Suzuki, N. Miyoshi, S. Matsumoto, T. Tanizawa, T. Tanaka, S. Tateishi, K. Kasahara, Catal. Today 27 (1996) 63.
[2] H. Mahzoul, J.F. Brilhac, P. Gilot, Appl. Catal. B 20 (1999) 47.
[3] E. Fridell, H. Persson, B. Westerberg, L. Olsson, M. Skoglundh, Catal. Lett. 66 (2000) 71.
[4] L. Olsson, H. Persson, E. Fridell, M. Skoglundh, B. Andersson, J. Phys. Chem. B 105 (2001) 6895.
[5] L. Olsson, E. Fridell, M. Skoglundh, B. Andersson, Catal. Today 73 (2002) 263.
[6] L. Lietti, P. Forzatti, I. Nova, E. Tronconi, J. Catal. 204 (2001) 175.
[7] K. Iwachido, H. Tanada, T. Watanabe, N. Yamada, O. Nakayama, H. Ando, M. Hori, S. Taniguchi, N. Noda, F. Abe, SAE Technical Paper, 2001-01-1298.
[8] T. Maunula, A. Vakkilainen, R. Heikkinen, M. Härkönen, SAE Technical Paper, 2001-01-3665.
[9] P. Engström, A. Amberntsson, M. Skoglundh, E. Fridell, G. Smedler, Appl. Catal. B 22 (1999) L241.
[10] H.Y. Huang, R.Q. Long, R.T. Yang, Appl. Catal. B 33 (2001) 127.
[11] T. Kirchner, G. Eigenberger, Chem. Eng. Sci. 51 (1996) 2409.
[12] G. Koltsakis, P. Konstantinidis, A. Stamanelos, Appl. Catal. B 12 (1997) 161.
[13] L. Olsson, B. Westerberg, H. Persson, E. Fridell, M. Skoglundh, B. Andersson, J. Phys. Chem. B 103 (1999) 10433.
[14] J. Jirát, M. Kubíček, M. Marek, Catal. Today 53 (1999) 583.
[15] S. Kojima, N. Baba, S. Matsunaga, K. Senda, K. Katoh, T. Itoh, SAE Technical Paper, 2001-01-1297.
[16] T. Bunluesin, R. Gorte, G. Graham, Appl. Catal. B 15 (1998) 107.
[17] J. Barbier, D. Duprez, Appl. Catal. B 4 (1994) 105.
[18] W. Press, S. Teukolsky, W. Vetterling, B. Flannery, Numerical Recipes in C, Cambridge University Press, Cambridge, 1994, p. 408.
[19] P. Aghalayam, Y. Park, D. Vlachos, AIChE J. 46 (2000) 2017.
[20] S. van der Linde, T. Nijhuis, F. Dekker, F. Kapteijn, J. Moulijn, Appl. Catal. A 151 (1997) 27.
[21] R. Jahn, D. Šnita, M. Kubíček, M. Marek, Catal. Today 70 (2001) 393.
[22] J. Jirát, M. Kubíček, M. Marek, Chem. Eng. Sci. 56 (2001) 1597.